

Original Article

Cite this article: Hesse R, Fong C, and Schumann D (2019) Origin of spherulitic and cone-in-cone concretions in Cambro-Ordovician black shales, St Lawrence Estuary, Quebec, Canada. *Geological Magazine* **156**: 1793–1804. <https://doi.org/10.1017/S0016756819000128>

Received: 22 March 2018
Revised: 28 January 2019
Accepted: 4 February 2019
First published online: 4 June 2019

Keywords:

concretions; spherulites; cone-in-cone structure; fibrous calcite-quartzine intergrowth; diagenesis; Cambro-Ordovician; Quebec

Author for correspondence: Reinhard Hesse, Email: reinhard.hesse@mcgill.ca

Origin of spherulitic and cone-in-cone concretions in Cambro-Ordovician black shales, St Lawrence Estuary, Quebec, Canada

Reinhard Hesse^{1,2,*} , Christopher Fong³ and Dirk Schumann⁴

¹Earth and Planetary Sciences, McGill University, 3450 University Street, Montreal, QC, H3A 0E8, Canada; ²Department of Earth- and Environmental Sciences, Section Geology, Faculty of Geosciences, Ludwig-Maximilians-Universität München, Luisenstraße 37, 80333, Munich, Germany; ³Apt. 5-1, 5th fl., No.417, Minquan Road, North District, Taihong, Taiwan and ⁴fibics Inc., 1431 Merivale Road, Suite 100, Ottawa, ON K2E 0B9, Canada

Abstract

Spherulitic concretions are very rare among carbonate concretions that generally consist of micritic carbonate. The occurrence of spherulitic concretions in Cambro-Ordovician black shales of unknown stratigraphic age on a mid-channel island in the St Lawrence Estuary in Quebec is a new example in addition to only three hitherto reported occurrences of spherulitic carbonate concretions. Their origin is still poorly understood. These concretions occur in close association with, and show various transitions to, cone-in-cone structure. The spherules, measuring 0.5 to 12 mm in diameter, consist of intergrown fine fibres of ferroan calcite and quartzine, pointing to the formation of the concretions below the sulfate-reduction zone. A phenomenological theory of spherulitic crystallization relates the thickness δ of an impurity-rich layer in front of impurity-rejecting growing crystals to the impurity-diffusion coefficient D and the growth velocity G of the crystal by $\delta = D/G$. In spherulite-forming environments, extremely small values of δ (in the order of $<10^{-4}$ cm) in conjunction with cellulation lead to spherulitic fibre growth. The theory of spherulitic crystallization is here applied to sedimentary deposits for the first time. The intimate association of calcite and quartzine in the concretions requires a chemical change from alkaline to acidic conditions, which occurs below the carbonate-reduction zone owing to the dissolution of sponge spicules or radiolarians. The transition from spherulite to the silica-free cone-in-cone structure occurs when the silica reservoir that acted as an impurity is exhausted in the crystallization process.

1. Introduction

Concretions, usually a minor sediment constituent by volume, are widespread in organic-matter-rich sediments and become a trademark of black shales, suggesting that the organic matter of black shales is the source of the carbonate in the concretions. The formation of concretions results from the early diagenetic bacterial decomposition of organic matter that leads to mineralization reactions, including carbonate precipitation (Daly, 1900; Bradford, 1916; Lalou, 1957; Hodgson, 1966, 1968; Berner, 1968, 1971; Franks, 1969; Curtis *et al.* 1972; Sass & Kolodny, 1972; Raiswell, 1976; Irwin *et al.* 1977; Curtis, 1978; Hudson, 1978). Carbonate concretions display a great variety in shape, internal structure(s) and chemical composition, and comprise three end-member groups according to their crystal habit: (1) micritic concretions consisting entirely of micrite calcite or dolomite crystals and lacking internal structure; (2) spherulitic carbonate concretions consisting of radiating fibrous calcite; and (3) cone-in-cone concretions and layers.

Most carbonate concretions show a spherical to ellipsoidal shape, being more or less flattened perpendicular to bedding, particularly in shaly host rocks. Diagenetic beds, elsewhere called sheet concretions (Pirrie & Marshall, 1991), result from the coalescence of individual concretions in concretion layers and are also either micritic, spherulitic or cone-in-cone.

Micritic concretions are generally early to very early diagenetic in origin, having been formed at a shallow burial depth of a few centimetres up to a few metres below seafloor (mbsf) (e.g. Hesse *et al.* 2004), although a few rare occurrences of much deeper formation (of up to 800 mbsf and 4 km burial depth, respectively) have been reported in the literature (von Rad & Botz, 1987; K. P. Polan, unpub. B.Sc. Honours thesis, McGill Univ., 1980). Concretions are very useful tools for unravelling the diagenetic history of the host rock (Raiswell, 1971, 1976; Oertel & Curtis, 1972; Sass & Kolodny, 1972; Curtis *et al.* 1975; Hudson, 1978; Hesse *et al.* 2004).

Concretions with cone-in-cone structure and their origin have been an intriguing subject of study for over a century (Sorby, 1859; Gresley, 1894; Tarr, 1921, 1922, 1932; Shaub, 1937; Usdowski, 1963; Durrance, 1965; MacKenzie, 1972). Cone-in-cone structures without a

© The Author(s), 2019. Published by Cambridge University Press. This is an Open Access article, distributed under the terms of the Creative Commons Attribution licence (<http://creativecommons.org/licenses/by/4.0/>), which permits unrestricted re-use, distribution, and reproduction in any medium, provided the original work is properly cited.



Fig. 1. Eastern Canada geography with Île-aux-Grues/Île-aux-Oies in the St Lawrence Estuary about 80 km northeast of Quebec City, Canada, shown as inset. Stars – sample locations; stippled area – tidal flats.

spherulitic association have been described by Brown (1954), Woodland (1964), Gilman & Metzger (1967), Franks (1969) and MacKenzie (1972), among others. Cone-in-cone structure is considered to be the result of low-nucleation rate precipitation, because unlike micritic carbonate in concretions, they push the clay of the host sediment aside during growth (Füchtbauer, 1971) and thus cannot be used to estimate palaeo-porosity at the time of precipitation. Prior to this study, all cone-in-cone structures were known to be composed of fine fibrous calcite or micritic calcite, the latter a product of recrystallization (Franks, 1969).

In contrast to the widespread occurrence of calcareous cone-in-cone structures, calcareous spherulitic carbonate concretions have rarely been reported in the literature (Allen, 1936; Muir & Walton, 1957; Hodgson, 1968), but have been produced experimentally (Morse *et al.* 1932; Morse & Donnay, 1936). Spherulitic concretions other than carbonates appear to be more common, especially in sideritic to rhodochrositic concretions (Spencer, 1925; Hewett, 1932; Deans, 1934; Stankevich, 1955; Chao & Davies, 1960; Miall, 1974; Browne & Kingston, 1993; Choi *et al.* 2003), phosphatic concretions (McConnell, 1935; Pecora *et al.* 1962; Shead, 1968) and monohydrocalcite (Stoffers & Fischbeck, 1974, 1975; Krumbein, 1975). A possible genetic relationship between spherulites and cone-in-cone structure was mentioned by Gilman & Metzger (1967). Hodgson (1968) observed the direct association of spherulites with cone-in-cone structure but did not elaborate on the genetic relationship between the two.

Carbonate concretions collected from a deep-water turbidite succession on the island of Île-aux-Grues/Île-aux-Oies exhibit a continuous transition between spherulitic and cone-in-cone concretion end-members. These concretions provide an insight into the mechanism of formation of spherulitic concretions and calcareous cone-in-cone structures and the transition from one into the other. Presenting this new example of spherulitic carbonate concretions and the interpretation of the mechanism of formation are the objectives of this contribution.

2. Geologic setting

The spherulitic and cone-in-cone concretions described here occur on Île-aux-Grues/Île-aux-Oies (Crane Island/Goose Island), a mid-stream island in the St Lawrence Estuary, 80 km northeast of Quebec City, Canada (Fig. 1), where the white Canadian geese stop over twice a year on their migration to and from the Arctic. The island is made up of a succession of Cambro-Ordovician turbidites and black shales of undetermined stratigraphic age. It consists of a lower unit of thin-bedded (less than 10 cm thick) spill-over turbidites (fine-grained sandstone and siltstone alternating with beds of black shale). Beds of this unit are in fault contact with higher stratigraphic units and are well exposed on the broad tidal flats that surround most of the island (Fig. 1, inset). A succession of red and green slumped siltstones follows the spill-over unit. Overlying the slump unit is another spill-over turbidite succession of fine sandstone and siltstone beds that alternate with thin beds of black shale. A number of channels occur throughout this unit. Channel-fill deposits at the top of the second spill-over turbidite represent the highest stratigraphic unit on the island. The carbonate concretions occur in the lower spill-over unit. They are usually arranged in layers following distinct stratigraphic horizons within the black shales. No correlation has been found between a particular type of concretion and the lithology of the host rocks.

3. Materials and methods

3.a. Sample preparation of extra-large thin-sections

Concretions were cut into equal halves and polished to reveal the fabric and structures. Extra-large thin-sections up to 8×12 cm were varnished with transparent lacquer for protection, since cover glasses of this size were unavailable. Scanning and direct photocopying by placing the smooth surface of a sample on the glass plate of a Xerox machine gave excellent images for study. Acetate peels were made from these concretions; however, their

size tended to cause the final peels to curl up into an unmanageable roll, rendering later observation difficult. The observations were made while the peels were initially still flat.

3.b. Etching to isolate silica and calcite

Etching using hydrofluoric acid for silica fibres and hydrochloric acid for calcite was performed on petrographic thin-sections as well as on polished surfaces. The results were satisfactory, since the two strong solvents did not react much with the shale materials enclosed within the cone-in-cone structures. Stereo-binoculars were used to study large cone-in-cone structures, whereas spherulites were studied under a petrographic microscope. Photomicrographs were taken and the area of observation was marked on the thin-section.

3.c. Large-area light microscopy

Large-area transmitted-light microscopy image mosaics were acquired from one large petrographic thin-section, using a Zeiss AXIO Zoom.V16 light microscope. The mosaics were acquired with the software ZEN Pro using the Plan Apo Z 0.5/0.125 objective (free working distance (FWD) 114 mm) at a resolution of 811 nm/pixel, both in plane-polarized light (PPL) and in cross-polarized light (XPL). The entire mosaic of the concretion consists of 772 image tiles.

3.d. XRD measurements

X-ray diffraction (XRD) measurements were carried out on a Siemens D500 powder diffractometer, using a $\text{CuK}\alpha$ source. Conditions of operation were 40 kV and 35 mA.

3.e. SEM analyses

A large-area scanning electron microscope (SEM) image mosaic of the part of the thin-section that was acid treated was acquired on a Zeiss EVO MA 15 tungsten filament SEM by using the Zeiss Atlas 5 software at Fibics Incorporated (Ottawa, Canada). The other half of the large thin-section was still covered with varnish and could therefore not be imaged in the SEM. The techniques described here have been developed based on the work of D. Schumann (unpub. Ph.D. thesis, McGill Univ., 2011).

The light microscopy mosaics (PPL, XPL) were imported into the Atlas 5 correlative workspace and aligned with the sample in the SEM. The exposed half of the thin-section was imaged with an accelerating voltage of 20 kV using simultaneously the backscattered electron (BSE) detector and the secondary electron detector (SE), with a working distance of 8.55 mm, a 1.4 nA beam current (30 μm aperture), a 3 μs dwell time and a resolution of 170 nm/pixel. The resulting two large-area mosaics (BSE and SE signals) comprise 3680 images, with each image tile consisting of 3072×3072 pixels ($521.5 \times 521.5 \mu\text{m}$), and a total pixel count of 34.7 gigapixels. Once the large-area image mosaic was acquired, stitched, corrected and properly aligned to the light microscopy mosaics (PPL, XPL), the entire Atlas 5 dataset was exported to an autonomous series of files called the Browser-Based Viewer (BBV). The BBV format allows anyone on a PC with a Web browser to look at the complete dataset at full resolution in a similar manner to that of the application Google Earth™. The computer mouse is used for zooming in and out as well as for navigating through the large-area image mosaic. The BBV datasets of the carbonate concretion can be viewed by following the link <https://www.petapixelproject.com/mosaics/RH/CC-BBV/Carbonate-Concretion/index.html>.

After the large-area SEM image mosaic was acquired, the Atlas 5 dataset was used to navigate to regions of interest for energy-dispersive spectroscopic (EDS) analyses. These EDS analyses were also carried out on the Zeiss EVO MA 15 tungsten filament SEM, which is equipped with two Bruker XFlash 6/30 energy-dispersive X-ray spectroscopy (EDS) detectors, which were controlled using the Esprit 1.9 software. An accelerating voltage of 20 kV and a 1.4 nA probe current were used for the acquisition of EDS element maps and point analyses. The acquired element maps and point analyses were exported from the Bruker Esprit software, arranged into figure plates using CoreDRAW X7, exported as PDF or JPG files, and linked with their respective location of acquisition in the Atlas 5 BBV dataset (<https://www.petapixelproject.com/mosaics/RH/CC-BBV/Carbonate-Concretion/index.html>). The analyses can be viewed by clicking with the mouse in the green rectangular regions that mark the locations in which the analyses were performed. After clicking, a new browser window will open and the PDF or the JPG file can be viewed and/or downloaded.

3.f. Carbon and oxygen stable isotope analyses

Samples from four spherulitic concretions were analysed for carbon and oxygen stable isotopes at the Université de Québec à Montreal. Data on $\delta^{13}\text{C}$ (Pee Dee Belemnite; PDB) and $\delta^{18}\text{O}$ (PDB) in calcite were acquired with a MAT-252 mass spectrometer. The extraction of CO_2 was done in a Carbonate Kiel Device III by Thermo Finnigan, which reproduces in an automated way the McCrea (1950) method. Carbonate is attacked with 100 % phosphoric acid at 70 °C. The reaction time is 3 minutes (calcite). The Carbonate Device is coupled to a MAT-252 isotope ratio mass spectrometer (Thermo Finnigan), in which the CO_2 produced is analysed. In order to evaluate the quality of the results, the NBS-19 international standard was used, with $\delta^{13}\text{C}$ (PDB) = +1.95 ‰ and $\delta^{18}\text{O}$ (PDB) = -2.20 ‰ values, certified by the IAEA. The standard deviation for the method used was 0.02 ‰ for $\delta^{13}\text{C}$ and 0.03 ‰ for $\delta^{18}\text{O}$. The standards NBS-19, calcite from a marble (carbonate of marine origin), and NBS-18, calcite from a carbonatite, were also used. The results were transformed as follows: $\delta^{18}\text{O VSMOW} = 1.03091 * \delta^{18}\text{O VPDB} + 30.91$ (Coplen, 1988).

4. Morphology and petrography of concretions

Among the three groups of carbonate concretions, the following distinctive types are recognized: (1) end-member micritic concretions; (2) transition of micritic concretions into spherulitic exterior shell (Fig. 2a); (3) micritic concretions with a cone-in-cone rind; (4) end-member spherulitic concretions (Fig. 2b); (5) spherulitic concretions with cone-in-cone rims; (6) end-member cone-in-cone concretions (Fig. 2c); (7) spherulitic lenses; (8) bedded cone-in-cone (Fig. 3a, b).

The concretions range in size from 7 to 40 cm in diameter. Thin beds of 'beef' cone-in-cone structures are usually laterally extensive (Fig. 3b). Spherulitic lenses reach a thickness of up to 20 cm and a length not exceeding 1 m.

Exposed surfaces of concretions or lenses reflect their internal structures. The surfaces of micritic concretions and those with a spherulitic rim are usually smooth. Spherulitic concretions are rather warty looking. This is the result of numerous spherules protruding irregularly a few millimetres beyond the surface into the host sediment (Fig. 4). Concretions with an outer shell of cone-in-cone structure invariably exhibit characteristic conic scales.

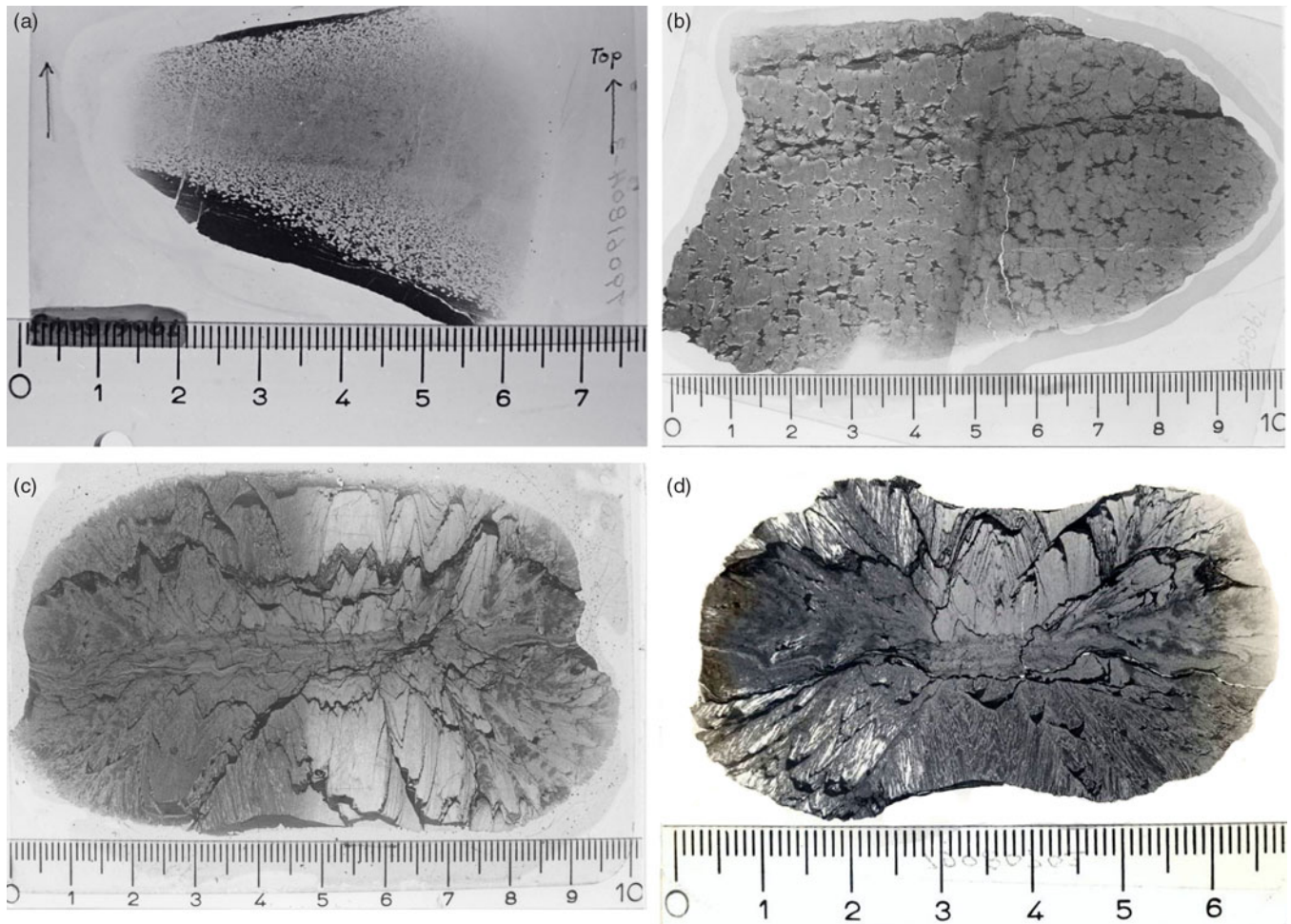


Fig. 2. (a) Transition of micritic concretion centre into exterior shell of spherules. (b) End-member spherulitic concretion. Two black shale seams occur in the upper half forming notches on the periphery of the concretion. Left half of thin-section is not stained. Numerous small cone-in-cone structures form rims on the spherules that appear light owing to their calcitic nature and absence of quartzine. (c) End-member cone-in-cone concretion. Left half of thin-section stained with Alizarin Red-S revealing the ferrous nature of the calcite. Note the uninterrupted zig-zag patterned seam of black shale that resulted from displacement by the growing cone-in-cone calcite structures. (d) End-member cone-in-cone concretion. Left half of thin-section: carbonate dissolved by HCl showing quartzine fibres (white). Scale in centimetres.

Furthermore, on both spherulitic and cone-in-cone concretions there are bedding-plane parallel notches that correspond to either a change from spherulitic to a cone-in-cone structure or a thin layer of silt or shale (Fig. 2b). Concretions composed entirely of cone-in-cone structure commonly are shaped like a jelly doughnut. The two polar regions may be depressed and underlain and overlain by black shale (Fig. 2d). On exposed vertical faces of bedded cone-in-cone structures, the characteristic ‘teepee’ forms are well exhibited as a result of differential weathering.

Seams and stringers of organic-matter-rich black shale and silt are common in the concretions. These seams are more or less straight and little affected by concretionary growth. Internal sedimentary structures of the host sediment, which include parallel lamination and rare small-scale ripple cross-lamination, are well preserved (Fig. 3b). In a few spherulitic concretions silt stringers inhibit the growth of spherules (Fig. 5a).

Under the microscope the spherules are composed of an intimate intergrowth of fine fibres of calcite and quartzine. The presence of fine silica fibres was not identified in XRD, but recognized in the larger-area SEM image mosaics and in the EDS analyses (Figs 6, 7, 8).

The SEM image mosaic allowed for the investigation of an entire half of a large concretion. The internal structure could be investigated at higher resolution and the chemistry of the components could be determined. The PPL image mosaic of the entire thin-section shows the various components of the carbonate concretion (Fig. 6; Atlas 5 BBV dataset <https://www.petapixelproject.com/mosaics/RH/CC-BBV/Carbonate-Concretion/index.html>). The carbonate appears pink in the stained area of the thin-section. The deformed shale bands appear as a brown to dark brown colour. The area of the thin-section that had undergone acid treatment was imaged with the SEM (Fig. 6). The area that was occupied with carbonate before that treatment now appears as black empty voids within the network of quartz fibres and deformed shale bands (Fig. 6; Atlas 5 BBV dataset <https://www.petapixelproject.com/mosaics/RH/CC-BBV/Carbonate-Concretion/index.html>). These areas appear white in PPL since the light is transmitted through the underlying thin-section glass and remaining glue that holds the actual thin-section (see Atlas 5 BBV dataset <https://www.petapixelproject.com/mosaics/RH/CC-BBV/Carbonate-Concretion/index.html>).

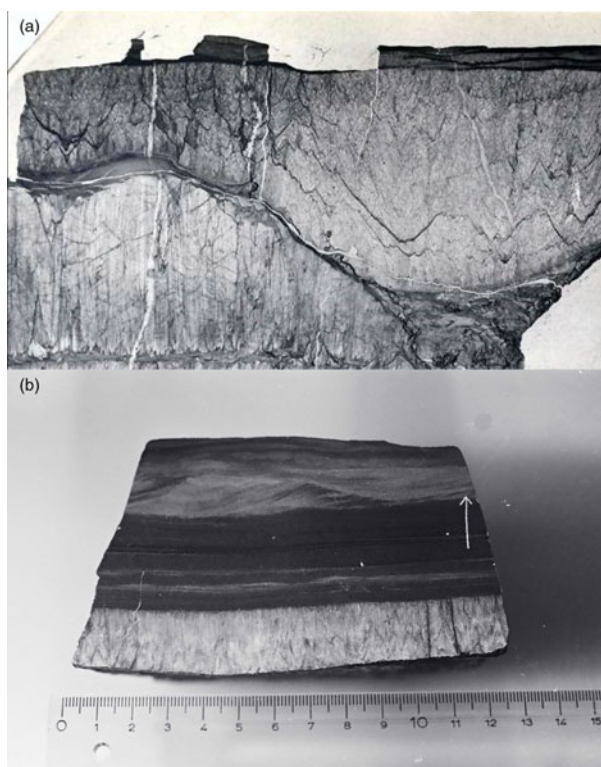


Fig. 3. (a) Two layers of cone-in-cone structure with a wavy boundary. The growth direction is inward. Thickness of the sample is c. 5 cm. (b) 'Beef' calcite cone-in-cone structure. Note cross-lamination in overlying fine sandstone bed. Scale in centimetres.



Fig. 4. 3D view of end-member spherulitic concretion showing a warty surface reflecting the make-up of the concretion by myriads of spherules. Scale: 30 cm.

The EDS element maps impressively show the distribution of the quartzine fibres and the deformed shale bands (Fig. 7; see also EDS maps in Atlas BBV dataset <https://www.petapixelproject.com/mosaics/RH/CC-BBV/Carbonate-Concretion/index.html>). A close investigation of the quartzine fibres reveals that they are formed of various shapes that look like casts of carbonate crystals and former cracks in the carbonate that were filled with quartzine, which were left behind after the carbonate was removed by etching with acid (Fig. 8a). The shale bands are composed of various types of phyllosilicates, chlorite, pyrite, quartz grains, titanium oxides, sodium feldspar, and in some cases xenotime (Fig. 8; see also linked EDS maps in the Atlas 5 BBV dataset <https://www.petapixelproject.com/mosaics/RH/>

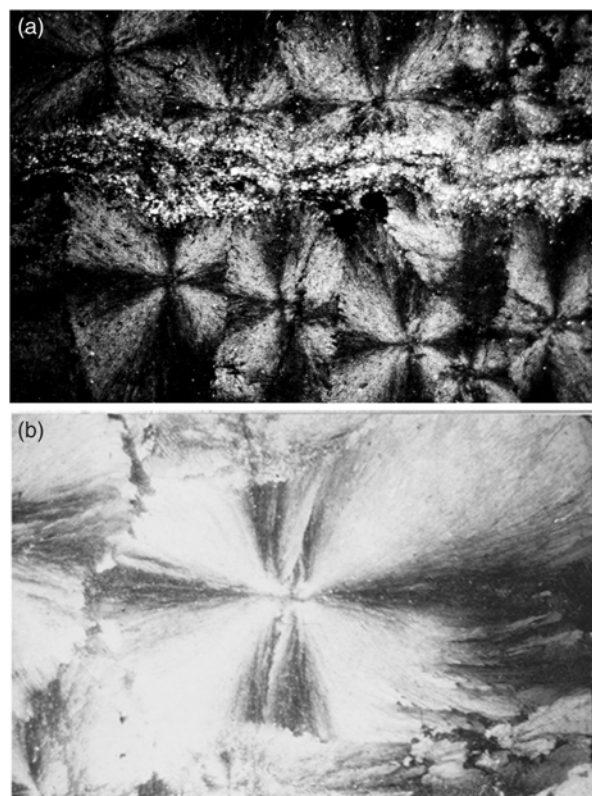


Fig. 5. (a) Silt stringers inhibiting the growth of spherules. Microscopic view under crossed nicols displaying the extinction cross in the radiating carbonate fibres of the spherules. Field of view is c. 1 cm wide. (b) Close-up of near-perfect spherical spherule with some compromise boundaries under crossed nicols showing extinction cross. Spherule is 2 mm in horizontal diameter.

[CC-BBV/Carbonate-Concretion/index.html](https://www.petapixelproject.com/mosaics/RH/CC-BBV/Carbonate-Concretion/index.html)). The carbonate to silica ratio in the spherules is c. 60:40; at the transition to the cone-in-cone structure, silica disappears.

Spherules in these carbonate concretions range in size from 0.5 mm to 12 mm in diameter. Spherules of larger size usually exhibit a perfect spherical shape (Fig. 5b), whereas medium- to small-sized spherules up to 3 mm in diameter are commonly tightly packed and may exhibit a shoebox shape as well as other irregular shapes (Fig. 9). The nuclei of the spherules are commonly very small and their identity cannot be deciphered. From the nuclei, numerous fine fibres of calcite and quartzine 2 to 6 μm in diameter radiate outwards. Under crossed nicols a characteristic black extinction cross is displayed by the spherules (Fig. 5). Within a given concretion, spherules in the same horizontal plane are usually of equal size. When adjoining spherules come into contact they share a compromise boundary (Fig. 9). Spherules with compromise boundaries depart in shape from the ideal spherical form. Spaces surrounding three or more spherules may be filled with patches of black shale that have been displaced into this space by the growth of the neighbouring spherules. In spherulitic concretions the total volume of black shale or silt is <20 %. At the contact between spherules and black shale a transition from spherule to cone-in-cone structure is commonly observed (Fig. 10). Where cone-in-cone structure follows the periphery of a spherule, the high concentration of quartzine fibres in the inner parts of the spherule is reduced and gives way to clear ferroan calcite (Fig. 11). Calcite in these cone-in-cone structures frequently exhibits distinctively curved twin lamellae and cleavages characteristic of fascicular optic

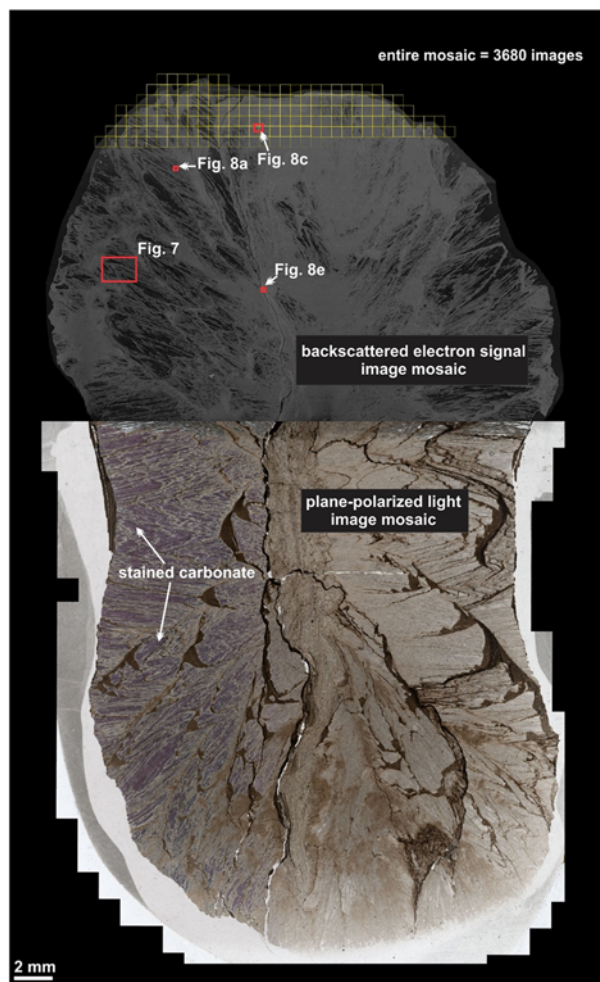


Fig. 6. Large-area image mosaic of the carbonate concretion showing the plane-polarized light image mosaic and the upper half from which a large-area Atlas 5 SEM (BSE) image mosaic was acquired.

and radiaxial mosaic (Kendall, 1985; Fig. 12a). In some cases, the cone-in-cone structure appears shaped like a bottle brush (Fig. 12b). The foregoing observations document the intimate relationship between the spherulitic and cone-in-cone structures.

In the present study, all of the examined cone-in-cone structures are made up of fine fibres of ferroan calcite. The smallest basic construction units in a cone-in-cone structure are slender conical tufts of fine fibres of calcite, which form various fan shapes with apical angles ranging from 15° to 70° (Figs 10, 11). The length of the fibrous tufts ranges from 0.5 to 15 mm. When three-dimensionally reconstructed, these slender conical tufts should be conical bundles of fine calcite fibres. The characteristic clay rings on cone-in-cone structures are the result of growth of fibrous tufts. As correctly interpreted by Franks (1969), the clay patches were pushed aside by the slender conical tufts until the clay patches butt against the sheaths of an earlier cone.

5. Carbon and oxygen stable isotopes

The carbon isotope values for the various types of concretions range from -28‰ to -7‰ (VPDB) (Fig. 13a); the oxygen values show a narrow spread between *c.* -17‰ and -9‰ (VPDB) with one runaway value of -29‰ (VPDB) (Fig. 13b).

6. Interpretation: mechanism of formation of spherules and cone-in-cone structures

Since the classic monograph of Bernauer (1929), who described experiments in which spherulitic growth was induced, a number of examples of successful experimental precipitation of fibrous spherules in the laboratory have been reported (Morse *et al.* 1932; Brooks *et al.* 1950; Heinisch, 1970; Schwartz *et al.* 1971; McCauley & Roy, 1974). As initially suggested by Bernauer, most authors attribute the precipitation of spherules to two factors: the presence of impurities and one form or another of a gel as the medium of crystallization.

Based on modern concepts of crystal growth, Keith & Padden (1963) developed a phenomenological theory of spherulite crystallization from a viscous magma, emphasizing the role of impurities in the spherulite-forming melt. Once impurities are added to a melt, the rate of advance of a crystallization front no longer depends upon the diffusion of latent heat away from the growth site alone, but rather upon an interplay between the transport of heat and the diffusion of impurities. The growing crystal rejects the impurities preferentially, and the concentration of the impurity in the liquid adjacent to the crystal builds up to higher than the average value in the melt. If the melt is not disturbed, an impurity-rich layer of 'thickness' $\delta = D/G$ forms in the liquid at the interface with the growing crystal, where D is the diffusion coefficient for the impurity in the melt, and G the growth velocity of the crystal. When the ambient temperature of the impurity-rich layer is smaller than the equilibrium liquidus temperature, small projections can be formed at the interface without additional latent heat having to be transported away. The surface of the growing crystal becomes broken up into numerous hexagonal cells. In this cellular crystallization, impurities are collected in the grooves between the hexagonal cells.

In a spherulite-forming melt, D values are reduced by several orders of magnitude, as evidenced by high melt viscosity. Together with very low G values, small δ values result (in most cases $<10^{-4}$ cm or $<1\ \mu\text{m}$). Since the equilibrium liquidus temperature gradient in the impurity-rich layer is steep, the surface of a hypothetical growing sphere is rendered extremely unstable, and cellular crystallization is to be expected. In the spherule-forming system, cellulation advances to an extreme and fibres grow rapidly on the sites of the hexagonal cells while impurities fill the grooves. In other words, the properties of spherulite-forming melts are such that the surface of a hypothetical growing spherule is forced to develop long fibrous projections separated one from another by uncrystallized melt. Owing to the lower temperature gradient in the impurity-rich layer, the uncrystallized melt will solidify slowly through secondary crystallization to fill in the overall structure. In this theory, Keith & Padden (1963) showed that the growth of fibrous crystals in spherulite-forming melts is attributable to cellulation and fibrillation on a fine scale, and brought about by a diffusive segregation of impurities in the manner described above.

Thus far, no consideration has been given to the curvature of the spherical surface and divergence of the cellular fibres. For the hypothetical growing sphere to complete its development into a spherulitic habit, the fibrous crystals should possess the ability to branch non-crystallographically at a small angle. The former authors stated that it is a fundamental property of cellular crystallization in an impure melt that any perturbation of the surface profile on a growing crystal is stable and persistent only if its size is commensurate with δ . Small disordered regions or minute singularities of the growing crystal have an opportunity to act as sources

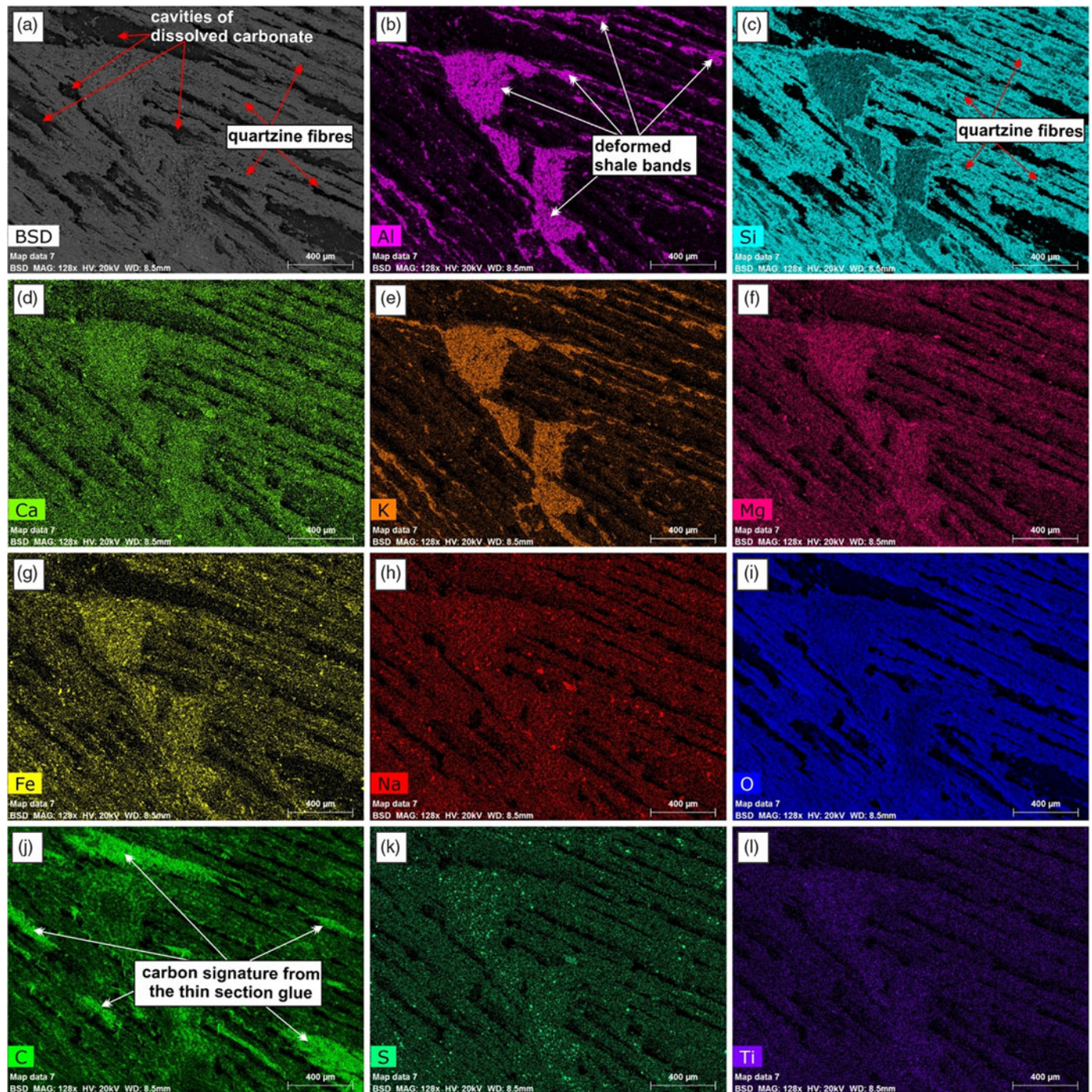


Fig. 7. Higher-magnification SEM-BSE images and EDS element maps of the part of the concretion from which the carbonate was removed showing the distribution of the quartz fibres and the deformed shale bands.

of persistent new growths only if δ is very small. Impure melts having high viscosities meet this condition. As δ is decreased from a relatively large value in such a melt, there is at first little likelihood of non-crystallographic branches being developed. As δ decreases, there is an increasing probability that one of the larger singularities at the shoulder of a growing fibre is of sufficient size that, with further growth, it becomes a persistent surface feature. If this new growth has a crystallographic orientation departing slightly from that of the parent fibres, it gives rise ultimately to a new fibre, which diverges from the original. Thus, one initial fibre has split into two

fibres, each about δ in width and each growing along the same preferred crystal axis but misaligned slightly with respect to the other. As δ decreases further, the probability of such an occurrence increases correspondingly and, when δ is very small, almost any island of surface disorder becomes a possible source of non-crystallographic branching. As far as branching is concerned, the essential difference between crystallization in simple liquids and in spherulite-forming melts is in the magnitude of δ . Only in spherulite-forming melts do sufficiently small diffusion coefficients exist to ensure values of δ that are small enough for branching to

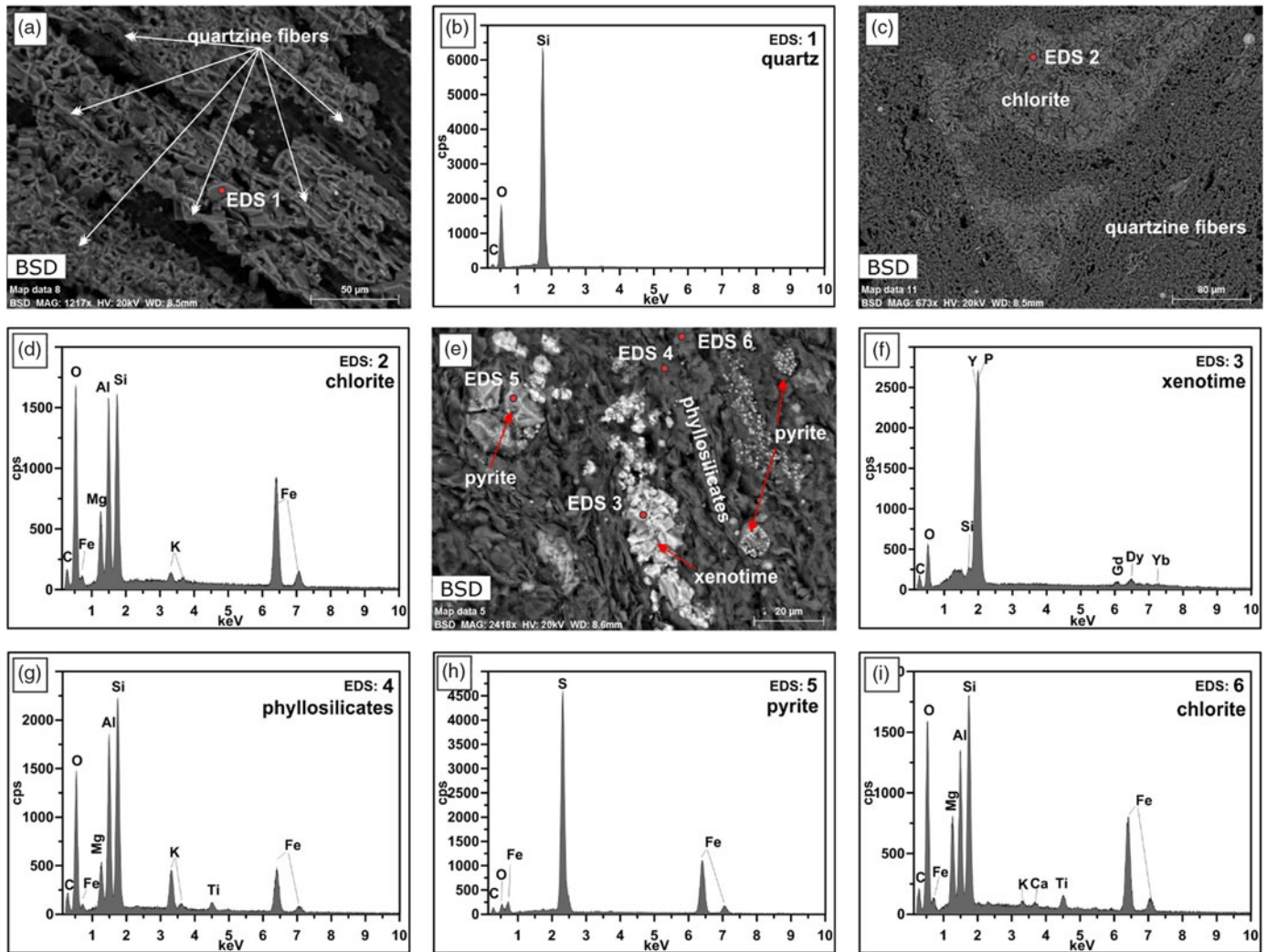


Fig. 8. (Colour online) Higher-magnification SEM-BSE images of the concretion. (a) Structure of the quartz fibers. (b) EDS point analyses of location 1 in (a). (c) Deformed part of a shale band consisting almost entirely of chlorite. (d) EDS point analyses of location 2 in (c). (e) Area in the shale that shows framboidal pyrite and xenotime. (f–i) EDS point analyses of locations 3 to 6 in (e).



Fig. 9. Tightly packed spherules with compromise boundaries.

become predominantly non-crystallographic. Keith & Padden (1963) observed that in polymers where δ was relatively large, spherules with coarse fibres and open textures were formed. Although the phenomenological theory of spherulite crystallization

was developed for melts, it should be applicable to precipitation from pore solutions in clastic sedimentary environments as it depends critically only on the numerical value of the δ parameter and the presence of two chemical species, where one represents an impurity that temporarily poisons the growing crystal surface.

The intimate association of quartzine and calcite in carbonate concretions from Île-aux-Grues/Île-aux-Oies at first sight seems hard to explain in terms of ordinary precipitation processes of these minerals. However, applying the phenomenological theory of Keith & Padden (1963), a convincing solution to the problem emerges.

Most spherules precipitated experimentally in the laboratory crystallized in a gelatinous medium in the presence of impurities. Silica gel is the most common medium used. The occurrence of silica gel has not been reported from clastic or biogenic siliceous pelagic deep-sea sediments (e.g. Hesse, 1990a,b), not even in hydrothermally sourced ponds of mid-ocean ridges like the Atlantic II Deep in the Red Sea. However, experimental spherulite precipitation has also been achieved from alkaline aqueous solutions (e.g. Johnston *et al.* 1916). Alkaline conditions are established

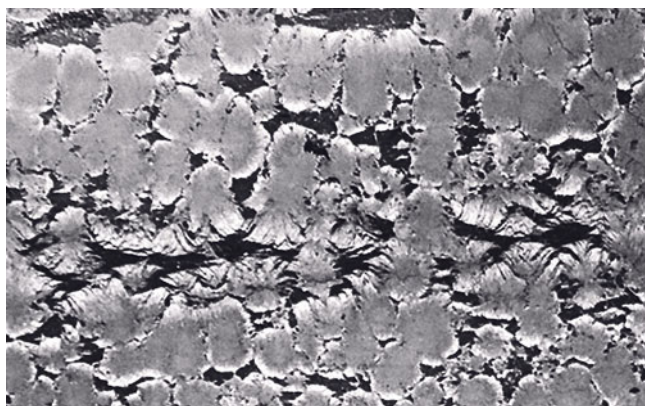


Fig. 10. Photomicrograph of cone-in-cone structure rimming spherules. The high concentration of quartzine fibres in the inner parts of the spherules is reduced and gives way to clear ferroan calcite in the rims of the spherules. Hand specimen 79072802-1. Horizontal width c. 36 mm.



Fig. 11. Close-up of cone-in-cone structure in the periphery of two spherules.

during early diagenesis in the lower sulfate-reduction zone (Hesse *et al.* 2004). If sufficient biogenic or detrital calcium carbonate has been dissolved in the oxidation zone, and the nitrate-reduction and upper sulfate-reduction zones where acidic conditions prevail, then fibrous calcium carbonate precipitation in the presence of impurities may start in the lower sulfate-reduction zone or the carbonate-reduction (methane generation) zone. The presence of ferroan calcite in the studied concretions speaks for the beginning of the precipitation in the carbonate-reduction zone, because in the sulfate-reduction zone Fe^{2+} is removed by sulfide and not available for incorporation into carbonate. The carbon isotope results (Fig. 13a) support an early diagenetic precipitation at the top of the methane-generating zone at a level where the effect of methane fractionation is still subordinate. (Note: C. Fong considers that precursor concretions formed at shallow subsurface depth, and their recrystallization leading to spherulitic and cone-in-cone structures occurred at depths in the order of 4 km after tectonic stacking.) No systematic variations between spherules (XB) and cone-in-cone structures (samples XC and XE) are recognizable. The oxygen isotope values would give temperatures too high even if a $\delta^{18}\text{O}$ of Early Palaeozoic seawater of $<-7\text{‰}$ is assumed (Fig. 13b; cf. Hesse *et al.* 2004). However, low $\delta^{18}\text{O}$ values may

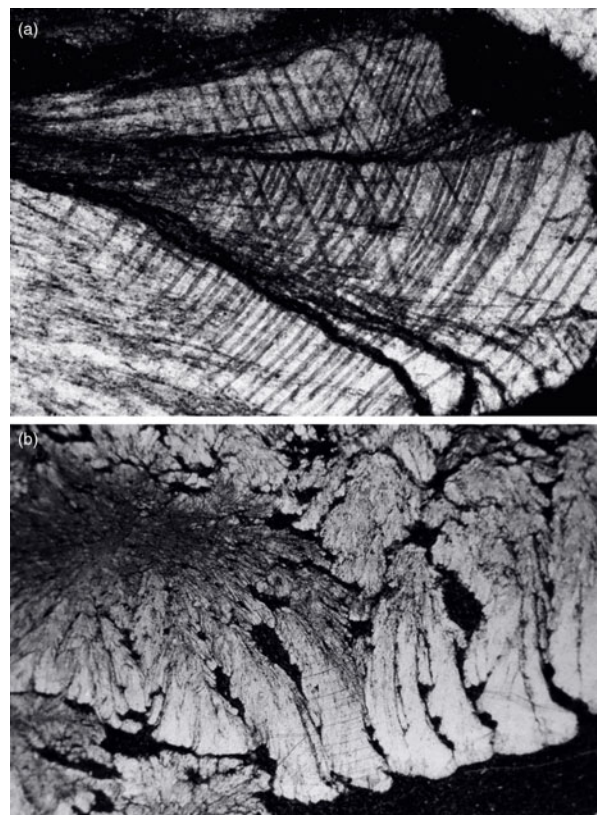


Fig. 12. (a) Calcite in cone-in-cone structure exhibiting distinctively curved twin lamellae and cleavages characteristic of fascicular optic and radiaxial mosaic (c.f. Kendall, 1985). (b) Cone-in-cone structure shaped like a bottle brush.

result from advection of pore waters from a greater subsurface depth (Hesse & Schacht, 2011).

Carbonate precipitation may occur alternating with silica precipitation, because carbonate crystallization lowers the pH (García-Ruiz *et al.* 2009). Under alkaline conditions dissolved silica is present, depending on pH, either as orthosilicic acid (H_4SiO_4) or in its dissociated forms $\text{H}_3\text{SiO}_4^{-1}$ (for $\text{pH} > 9$) or $\text{H}_2\text{SiO}_4^{2-}$ (for $\text{pH} > 13$). Dissociation raises the silica solubility significantly (Hesse, 1990a). Silica precipitation from supersaturated solutions involves polymerization in which monomeric acid first forms oligomers (dimers, tetramers, etc.) through the development of siloxane (Si–O–Si) bonds and then high-molecular-weight polymers (with molecular weights up to 10^2 – 10^3) which have colloidal dimensions (greater than 5 nm) and remain in suspension as sols unless precipitated as gels by metal hydroxides. The most commonly used hydroxide for silica precipitation in industrial applications is $\text{Mg}(\text{OH})_2$, also thought to be instrumental in the nucleation of opal-CT (Kastner *et al.* 1977). Presently known environments of inorganic silica precipitation are the playa lakes of the Coorong Lagoon, Australia, which have a pH of ~ 10 , Lake Bogoria in the Kenya Rift Valley (Renaut *et al.* 1986; Renaut & Owen, 1988) and others. Here the silica probably goes through a gel stage. Precipitation takes place when the pH drops owing to decaying plant matter during evaporation. Conditions of the shallow lacustrine environment of the Coorong Lagoon would not have been applicable to the continental slope setting of Laurentia in Cambrian or Ordovician times.

However, as pointed out, pH-lowering through carbonate precipitation would have triggered silica precipitation. The presence of

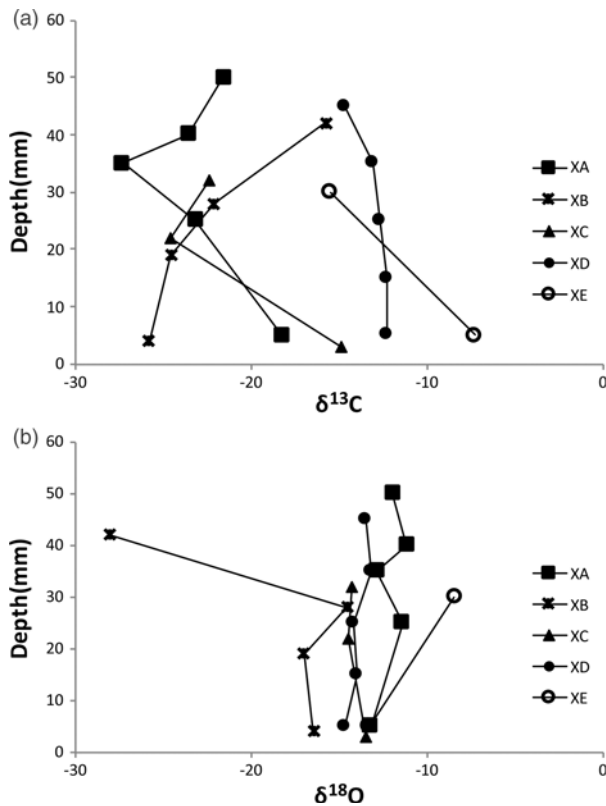


Fig. 13. (a) Carbon and (b) oxygen isotope traverses across five different types of spherulitic and cone-in-cone concretions. XA – spherules grading downwards into cone-in-cone structure; XB – spherulitic concretion; XC – cone-in-cone structure on rim of spherulitic concretion; XD – micritic concretion with spherule rim; XE – cone-in-cone concretion.

dissolved silica supplied by the dissolution of unstable biogenic opal-A (in Palaeozoic time provided by radiolarians and sponge spicules) during shallow burial leads to local supersaturation of silicic acid next to the growing carbonate crystals, initiating the adsorption and precipitation of silica on the positively charged carbonate crystal surfaces (Fig. 8a). Silica precipitation poisons carbonate crystal growth and causes bifurcation of the carbonate crystals. The chemical coupling of carbonate and silica precipitation enables continuous crystal splitting at non-crystallographic angles, thus producing the radiating spherulitic fibres. If the silica supersaturation in the pore water is low enough, direct precipitation of the silica as stable chaledony or quartzine is possible instead of the metastable precursor opal-CT phase.

In the concretions described, the cement (represented by the crystallized spherules) to solid ratio is as high as 80:20. The type of sediment at the depth of concretion growth is a soupy mud with high water content (Müller, 1967). The presence of calcite nuclei dictates that calcite is the initial mineral precipitated, while silica, although in excessively high concentration, constitutes the impurity attributed to the crystallization of fibrous calcite. The silica that filled interfibre grooves underwent secondary crystallization and formed a fibrous network. In well-formed and fully developed spherules, these silica fibres dominate the entire network, consequently obscuring the manner of calcite branching of the calcite fibres. Could the silica have been introduced by replacement as in the case of silica replaced cone-in-cone structures reported by Lugli *et al.* (2005)? This is next to impossible because of the fine fibrous intergrowth of ferroan calcite and silica in the spherules.

The rimming cone-in-cone structure should then also have been replaced by silica.

Observation under the petrographic microscope reveals that transition from spherule to cone-in-cone structure is brought about by an increase in the angle of branching of the fibres. Since the transition is accompanied by the disappearance of silica fibres from the structure as confirmed by the SEM/EDS analyses, it appears that exhaustion of the silica reservoir is the cause of the change from spherulitic to cone-in-cone structure.


According to Lugli *et al.* (2005), hypotheses concerning the formation of calcareous cone-in-cone structure belong to two groups: those assuming early displacive formation of concretions in soft, unconsolidated sediment, and those that emphasize late fracturing of concretions with or without excess pore fluid. In detail, the following hypotheses have been proposed (see also Mozley, 2003):

- (1) Recrystallization of fibrous aragonite to calcite forming open cone fractures intruded by argillaceous matter (Tarr, 1922; Gilman & Metzger, 1967).
- (2) Differential pressure solution on calcite fibres along conical shear planes induced by the weight of overlying strata (Tarr, 1932).
- (3) Settling and volume shrinkage during the slow dewatering of highly saturated and loosely packed subaerially exposed sediments (Shaub, 1937).
- (4) Precipitation of fibrous calcite along fractures or in concretionary masses. The fibres would then be deformed by 'tractional forces' during deformation of the host strata or during concretionary growth of the calcite component (Bonte *et al.* 1947).
- (5) Crystallization of calcite fibres under gravity-induced differential stress, during gradual compaction of the sediment. The angles of cone apices would be determined by the plasticity of the enclosing sediment: large apical angles would indicate relatively low plasticity (Woodland, 1964).
- (6) Early displacive growth of cone-shaped plumose aggregates of fibrous calcite (Franks, 1969).
- (7) Diagenetic water-escape structures promoting the 'reordering of phyllitic elements within a sediment undergoing diagenetic compaction and which exhibits differences in porosity and competency in its lithological composition; cone-in-cone can be compared to a schistosity acquired in the realm of hydroplastic deformation' (Becq-Giraudon, 1990).
- (8) Brittle fracturing of crystalline calcite aggregates, grown by a crack-seal mechanism in overpressured environments, and induced by a decrease in pore pressure of the plastic host sediment (Selles-Martinez, 1994).
- (9) Shallow burial (<1500 m) precipitation from modified marine pore fluids (Hendry, 2002).
- (10) Early diagenetic growth (depth <40 m), probably microbially mediated, in sandstone units beneath flooding surfaces and sequence boundaries (McBride *et al.* 2003).

7. Conclusions

The studied example of spherulitic carbonate concretions is only the fourth occurrence reported in the literature and the first example of an entire concretion documented by a large-area image mosaic dataset. The concretions occur in close association with cone-in-cone structure and show all transitions between end-member spherulitic concretions and cone-in-cone structure, with cone-in-cone forming towards the margins of individual spherules.

Detailed petrographic analyses have shown that the spherules consist of an intergrowth of ferrous carbonate and quartzine fibres. The significance of the detection of the quartzine is that it is a key factor for the understanding of spherulitic growth. Silica in solution acts as an impurity that is the cause for spherulitic growth, as predicted by the theory of Keith & Padden (1963) that was developed for spherulitic crystallization from magmas and has been applied in this study for the first time to sedimentary deposits, i.e. the growth of spherulitic carbonate concretions. The transition from spherules to cone-in-cone occurs when the reservoir of dissolved silica that acted as an impurity is exhausted.

Author ORCIDs.  Reinhard Hesse, 0000-0002-6430-6186

Acknowledgements. We are grateful to Robert F. Martin and Jeanne Paquette for providing important references. Journal reviewer Kyungsik Choi and an anonymous reviewer are thanked for constructive criticism of the manuscript. The study was financially supported by grants from the Natural Sciences and Engineering Research Council of Canada (NSERC).

References

- Allen VT (1936) A mineralized spherulitic limestone in the Cheltenham Fireclay. *American Mineralogist* **21**, 369–73.
- Becq-Giraudon JF (1990) La structure cone in cone en milieu de depot siliclastique; observations nouvelles sur les cone in cone de l'Ordovicien inferieur de la Montagne Noire, sud du Massif central français. *Geologie de la France* **1990** (2), 11–20.
- Bernauer F (1929) *Gedrilte Kristalle*. Berlin: Bornträger, 102 pp.
- Berner RA (1968) Calcium carbonate concretion formed by the decomposition of organic matter. *Science* **159**, 195–7.
- Berner RA (1971) *Principles of Chemical Sedimentology*. New York: McGraw Hill, 240 pp.
- Bonte A, Denaeyer ME and Goguel J (1947) Les facteurs mecaniques dans la genese de la structure "cone-in-cone". *Compte Rendu Sommaire des Seances de la Societe Geologique de France* **9**, 182–4
- Bradford SC (1916) The Liesegang phenomenon and concretionary structures in rocks. *Nature* **97**, 80–1.
- Brooks R, Clarke LN and Thurston EF (1950) Calcium carbonate and its hydrates. *Philosophical Transactions of the Royal Society of London A* **243**, 145–67.
- Brown R (1954) How does cone-in-cone material become emplaced? *American Journal of Science* **252**, 372–6.
- Browne GH and Kingston DM (1993) Early diagenetic spherulitic siderites from Pennsylvanian paleosols in the Boss Point Formation, Maritime Canada. *Sedimentology* **40**, 467–74.
- Chao ECT and Davies WE (1960) Authigenic rhodochrosite spherules from Gardner Creek, Kentucky. *United States Geological Survey Professional Paper* **400B**, 446–7.
- Choi KS, Khim BK and Woo KS (2003) Spherulitic siderite in the Holocene coastal deposits of Korea (eastern Yellow Sea), elemental and isotopic composition and depositional environment. *Marine Geology* **202**, 17–31.
- Coplen TB (1988) Normalization of oxygen isotope data. *Chemical Geology: Isotope Geoscience Section* **72** (4), 293–7.
- Curtis CD (1978) Possible links between sandstone diagenesis and depth related geothermal reactions occurring in enclosing mudstones. *Journal of the Geological Society, London* **135**, 107–17.
- Curtis CD, Petrowski C and Oertel G (1972) Stable carbon isotope ratios within carbonate concretions: a clue to time and place of origin. *Nature* **235**, 98–130.
- Curtis CD, Somogyi VA and Pearson MJ (1975) Mineralogy, chemistry and origin of a concretionary siderite sheet (clay ironstone band) in the Westphalian of Yorkshire. *Mineralogical Magazine* **40**, 385–93.
- Daly RA (1900) The calcareous concretions of Kettle Point, Lambton County, Ontario. *Journal of Geology* **8**, 135.
- Deans T (1934) The spherulitic ironstones of West Yorkshire. *Geological Magazine* **71**, 49–65.
- Durrance EM (1965) Cone-in-cone structures: a new interpretation. *Proceedings of the Geologists' Association* **76**, 83–90.
- Franks PC (1969) Nature, origin and significance of cone-in-cone structures in the Kiowa Formation (Early Cretaceous), North-Central Kansas. *Journal of Sedimentary Petrology* **39**, 1438–54.
- Füchtbauer H (1971) Cone-in-cone, a low-nucleation cement in marls. In *Carbonate Cements* (ed. CP Bricker), pp. 193–5. The John Hopkins University Studies in Geology 19. Baltimore: John Hopkins Press.
- García-Ruiz JM, Melero-García E and Hyde ST (2009) Morphogenesis of self-assembled nanocrystalline materials of barium carbonate and silica. *Science* **323**, 362–5.
- Gilman RA and Metzger WJ (1967) Cone-in-cone concretions from western New York. *Journal of Sedimentary Petrology* **37**, 87–95.
- Gresley WS (1894) Cone-in-cone: how it occurs in the Devonian Series in Pennsylvania, U.S.A., with further details of its structure, varieties, etc. *The Quarterly Journal of the Geological Society of London* **50**, 731–9.
- Heinisch HK (1970) *Crystal Growth in Gels*. University Park, Pennsylvania: The Pennsylvania State University Press, 111 pp.
- Hendry JP (2002) Geochemical trends and palaeohydrological significance of shallow burial calcite and ankerite cements in Middle Jurassic strata on the East Midlands Shelf (onshore UK). *Sedimentary Geology* **151**, 149–76.
- Hesse R (1990a) Origin of chert I. Diagenesis of biogenic siliceous sediments. In *Diagenesis* (eds IA McIlreath and DW Morrow), pp. 227–51. *Geoscience Canada Reprint Series* **4**.
- Hesse R (1990b). Pore-water anomalies in gas-hydrate bearing sediments of the deeper continental margins: facts and problems. *Journal of Inclusion Phenomena Molecular Recognition in Chemistry* **8**, 117–38.
- Hesse R. and Schacht U (2011) Early diagenesis of deep-sea sediments. In *Deep-Sea Sediments* (eds H Hüenecke and T Mulder), pp. 577–713. *Developments in Sedimentology* Vol. 63. Amsterdam: Elsevier.
- Hesse R, Shah J and Islam S (2004) Physical and chemical growth conditions of Ordovician organogenic deep-water dolomite concretions: implications for the $\delta^{18}\text{O}$ of Early Palaeozoic sea water. *Sedimentology* **51**, 601–25.
- Hewett DF (1932) Manganese in sediments. In *Treatise on Sedimentation* (ed. WH Twenhofel), pp. 562–81. Baltimore: The Williams and Wilkins Co.
- Hodgson WA (1966) Carbon and oxygen isotope ratios in diagenetic carbonates from marine sediments. *Geochimica et Cosmochimica Acta* **30**, 1223–33.
- Hodgson WA (1968) The diagenesis of spherulitic concretions and other rocks from Mangakahia Group sediments, Kaipara Harbour, New Zealand. *Journal of Sedimentary Petrology* **38**, 1254–63.
- Hudson JD (1978) Concretions, isotopes, and the diagenetic history of the Oxford Clay (Jurassic) of Central England. *Sedimentology* **25**, 338–70.
- Irwin H, Curtis CD and Coleman M (1977) Isotopic evidence for source of diagenetic carbonate formed during burial of organic-rich sediments. *Nature* **269** (5625), 209–13.
- Johnston J, Merwin HE and Williamson ED (1916) The several forms of calcium carbonate. *American Journal of Science*, 4th Series **41**, 473–512.
- Kastner M, Keene JB and Gieskes JM (1977) Diagenesis of siliceous oozes. I. Chemical controls on the rate of opal-A to opal-CT transformation – an experimental study. *Geochimica et Cosmochimica Acta* **41**, 1041–59.
- Keith HD and Padden FJ Jr (1963) A phenomenological theory of spherulite crystallization. *Journal of Applied Physics* **34**, 2407–21.
- Kendall AC (1985) Radial fibrous calcite: a reappraisal. In *Carbonate Cements* (eds N Schneidermann and PN Harris), pp. 50–79. Society of Economic Paleontologists and Mineralogists Special Publication 36.
- Krumbein WB (1975) Biogenic monohydrocalcite spherules in lake sediments of Lake Kivu (Africa) and Solar Lake (Sinai). *Sedimentology* **22**, 631–4.
- Lalou C (1957) Studies on bacterial precipitations of carbonates in sea water. *Journal of Sedimentary Petrology* **27**, 190–5.
- Lugli S, Reimold WU and Koeberl C (2005) Silicified cone-in-cone structures from Erfoud (Morocco): a comparison with impact-generated shatter cones. In *Impact Tectonics* (eds C Koeberl and H Henkel), pp. 50–65. Berlin: Springer.
- MacKenzie WS (1972) Fibrous calcite, a middle Devonian geologic marker, with stratigraphic significance. District of Mackenzie, Northwest Territories. *Canadian Journal of Earth Sciences* **9**, 1431–40.

- McBride EF, Picard MD and Milliken KL** (2003). Calcite-cemented concretions in Cretaceous sandstone, Wyoming and Utah, U.S.A. *Journal of Sedimentary Research* **73**, 462–84
- McCauley JW and Roy R** (1974) Controlled nucleation and crystal growth of various CaCO₃ phases by silica gel technique. *American Mineralogist* **59**, 947–63.
- McConnell D** (1935) Spherulitic concretions of dahllite from Ishawooa, Wyoming. *American Mineralogist* **20**, 693–8.
- McCrea JM** (1950) On the isotopic chemistry of carbonates and a paleotemperature scale. *The Journal of Chemical Physics* **18**, 849–57.
- Miall AD** (1974) Manganese spherulites at an intra-Cretaceous unconformity, Banks Island, Northwest Territories. *Canadian Journal of Earth Sciences* **11**, 1704–16.
- Morse HW and Donnay JDH** (1936) Optics and structure of three dimensional spherulites. *American Mineralogist* **21**, 391–426.
- Morse HW, Warren CH and Donnay JDH** (1932) Artificial spherulites and related aggregates. *American Journal of Science* **23**, 421–39.
- Mozley P** (2003) Diagenetic structures. In *Encyclopedia of Sediments and Sedimentary Rocks* (eds GV Middleton, MJ Church, M Coniglio, LA Hardie and FJ Longstaffe), pp. 219–225. Dordrecht: Kluwer Academic Publishers.
- Muir RO and Walton EK** (1957) The East Kirkton Limestone. *Transactions of the Geological Society of Glasgow* **22**, 157–68.
- Müller G** (1967) Diagenesis in argillaceous sediments. In *Diagenesis in Sediments* (eds G Larsen and GV Chilingar), pp. 127–77. Developments in Sedimentology Vol. 8. Amsterdam: Elsevier.
- Oertel G and Curtis CD** (1972) Clay-ironstone concretions preserving fabrics due to progressive compaction. *Geological Society of America Bulletin* **83**, 2597–606.
- Pecora WT, Hearn BC Jr and Milton C** (1962) Origin of spherulitic phosphate nodules in basal Colorado Shale, Bearpaw Mountains, Montana. *United States Geological Survey Professional Paper* **1962**, B30–35.
- Pirrie D and Marshall JD** (1991) Field relationships and stable isotope geochemistry of concretions from James Ross Island, Antarctica. *Sedimentary Geology* **71**, 137–50.
- Raiswell R** (1971) The growth of Cambrian and Liassic concretions. *Sedimentology* **17**, 147–71.
- Raiswell R** (1976) The microbiological formation of carbonate concretions in the Upper Lias of NE England. *Chemical Geology* **18**, 227–44.
- Renaut RW and Owen RB** (1988) Opaline silica associated with sublacustrine hydrothermal springs at Lake Bogoria, Kenya Rift Valley. *Geology* **16**, 699–702.
- Renaut RW, Tiercelin JJ and Owen RB** (1986) Mineral precipitation and diagenesis in the sediments of Lake Bogoria basin. Kenya Rift Valley. In *Sedimentation in the African Rifts* (eds LE Frostic, RW Renaut, I Reid and JJ Tiercelin), pp. 159–75. Geological Society of London, Special Publication no. 25.
- Sass E and Kolodny Y** (1972) Stable isotopes, chemistry and petrology of carbonate concretions (Mishash Formation, Israel). *Chemical Geology* **10**, 261–86.
- Schwartz A, Eckart D, O'Connell J and Francis K** (1971) Growth of vaterite and calcite crystals in gels. *Materials Research Bulletin* **6**, 1341–4.
- Selles-Martinez J** (1994) New insights in the origin of cone-in-cone structures. *Carbonates and Evaporites* **9**, 172–86.
- Shaub BM** (1937) The origin of cone-in-cone and its bearing on the origin of concretions and septaria. *American Journal of Science*, 5th Series **34**, 331–44.
- Shear A** (1968) Spherulites in the phosphatic concretions of the Woodford Chert, Arbuckle Mountains, Oklahoma. *Oklahoma Academy of Science* **47**, 171–2.
- Sorby HC** (1859) On the origin of “cone-in-cone”. In *Report of the 29th Meeting of the British Association for the Advancement of Science, 1859, Transactions of the Sections, Geology*, pp. 124. London: John Murray.
- Spencer E** (1925) On some occurrences of spherulitic siderite and other carbonates in sediments. *Quarterly Journal of the Geological Society of London* **81**, 667–705.
- Stankevich LO** (1955) Calciferous rhodochrosite from the Kerch deposits. *Doklady Akademii Nauk SSSR* **105**, 1328–31 (in Russian).
- Stoffers PE and Fischbeck R** (1974) Monohydrocalcite in lake sediments of Lake Kivu (East Africa). *Sedimentology* **21**, 163–70.
- Stoffers PE and Fischbeck R** (1975) Biogenic monohydrocalcite spherules in lake sediments of Lake Kivu (Africa) and the Solar Lake (Sinai): a reply. *Sedimentology* **22**, 635–6.
- Tarr WA** (1921) Syngeneric origin of concretions. *Geological Society of America Bulletin* **32**, 373–84.
- Tarr WA** (1922) Cone-in-cone. *American Journal of Science*, 5th Series **4**, 199–213.
- Tarr WA** (1932) Cone-in-Cone. In *Treatise on Sedimentation* (ed. WH Twenhofel), pp. 716–33. Baltimore: The Williams and Wilkins Co.
- Udowski HE** (1963) Die Genese der Tutenmergel oder Nagelkalke (cone-in-cone). *Beiträge zur Mineralogie und Petrographie* **9**, 95–110.
- von Rad U and Botz R** (1987) Authigenic Fe–Mn carbonates in the Cretaceous and Tertiary continental rise sediments of Deep Sea Drilling Project Site 603 off the eastern U.S.A. In *Initial Reports of the Deep Sea Drilling Project, vol. 93* (eds JE van Hinte SW Jr. Wise, BNM Biart, JM Covington, DA Dunn, JA Haggerty, MW Johns, PA Meyers, MR Moullade, JP Muza, JG Ogg, M Okamura, M Sarti and U von Rad), pp. 1061–71. Washington, D.C.: U.S. Government Printing Office.
- Woodland BG** (1964) The nature and origin of cone-in-cone structure. *Fieldiana: Geology* **13**, 185–305.